Chinese Journal of Chemical Engineering 47 (2022) 71–78

Contents lists available at ScienceDirect

Chinese Journal of Chemical Engineering

journal homepage: www.elsevier.com/locate/CJChE

Full Length Article

Enhancement of acetylene and ethylene yields in partially decoupled oxidation of ethane by changing the composition of heat carrier

Tianpeng LiZhou, Jiajia Luo, Tiefeng Wang *

Beijing Key Laboratory of Green Reaction Engineering and Technology, Department of Chemical Engineering, Tsinghua University, Beijing 100084, China

ARTICLE INFO

Article history:
Received 17 April 2021
Received in revised form 14 June 2021
Accepted 4 July 2021
Available online 28 July 2021

Keywords:
Partially decoupled process (PDP)
Ethane
Computational fluid dynamics (CFD)
Steam addition

ABSTRACT

In our previous work, a partially decoupled process (PDP) was proposed for efficient conversion of ethane to increase the ethylene yield and a new structural reactor called forward-impinging-back reactor (FIB) was proposed for scale-up. In this work, the influence of changing the composition and temperature of the heat carrier was investigated by simulations with detailed chemistry to further increase of the C_2 (C_2H_2 + C_2H_4) yield in the PDP of ethane. At ideal mixing conditions, the C_2 yield is 75.3% without steam addition and it is 82.9% at steam addition ratio of β = 1.4. In comparison, the C_2 yield in an FIB reactor is 62.4% without steam addition and it increases to 78.5% with steam addition (β = 1.4). The requirement of high mixing efficiency is diminished by steam addition, which is favorable for reactor scale-up.

1. Introduction

As the problems of climate change and global warming become severe, extensive research has focused on the use of natural gas as energy resource. Compared to coal and oil, natural gas can reduce CO_2 emission [1]. It is anticipated that a large portion of natural gas will be supplied by shale gas, tight gas, and coal bed methane [1]. With the advances in the technologies of drilling horizontal wells and multistage hydraulic fracturing [2,3], the production of shale gas has increased greatly in recent years [4]. Also, the dramatic rising of shale gas has made it a dominant source of energy in some places, and has a great influence on the world gas supply chains [5–10]. Shale gas contains a considerable amount of ethane [4], which is used as feedstock for production of chemicals.

As one of the most important raw materials, olefins are produced by catalytic or thermal cracking of hydrocarbons, such as ethane, propane, and naphtha [11]. At present, ethane is mainly used as the feedstock of steam cracking process for producing C_2H_4 with ~52% C_2H_4 yield at 65% C_2H_6 conversion [12]. Although the steam cracking process has a high selectivity to C_2H_4, it is energy consuming due to its low one-pass conversion [13]. The catalytic oxidative dehydrogenation is another potential approach to convert ethane to ethylene, with an ethylene yield of 40%–75% [14–19]. However, severe catalyst deactivation limits the industrial applications of the oxidative dehydrogenation process.

In our previous work, based on in-depth analysis of the methane partial oxidation (POX) process, a new process named partially decoupled process (PDP) was proposed, which separates the oxidation and pyrolysis reactions by a special reactor design [20,21]. In the PDP, the proportion of methane and ethane consumed by combustion for heat supply can be replaced by other cheap fuel gases such as coke oven gas. The fuel gas combusts with stoichiometric oxygen to generate heat carrier, and the ethane or methane feedstock is mixed with the heat carrier and undergoes pyrolysis at a high temperature. Simulations with detailed chemistry show that the maximum C_2 (C_2H_2 + C_2H_4) yield is 65% at 97% ethane conversion in the ethane PDP. In the validation experiments, the C_2 yield reached 52% at 70% ethane conversion [22], confirming that the PDP is at least comparable to the ethane steam cracking process in ethylene yield. In order to solve the scale-up problem of the jet-in-cross-flow (JICF) reactor, a new reactor named forward-impinging-back (FIB) reactor was proposed for scaling up the PDP [23]. The C_2 yield of ethane PDP only decreased from 64.4% to 63.8% in a FIB reactor when reactor diameter is scaled up from 30 mm to 390 mm, which is much better than the JICF reactor.

The heat carrier of the ethane PDP in our previous work was set as coke oven gas combusted with stoichiometric oxygen. Since the high calorific value of coke oven gas, the temperature of heat carrier could reach 3100 K. The excessively high temperature of heat carrier promotes the homolysis of ethane and formation of CH_4. In addition, H_2O molecules split into H and OH radicals, and CO_2 molecules split into CO and O radicals. The target products, C_2H_2

* Corresponding author.
E-mail address: wangtf@tsinghua.edu.cn (T. Wang).

https://doi.org/10.1016/j.cjche.2021.07.012
1004-9541/

and C_2H_4, will be oxidized by the oxidative radicals, causing a decrease in C_2 yield. Therefore, the C_2 yield is expected to further increase by decreasing the temperature of heat carrier. The stability of CO_2 and H_2O molecules is different at high temperatures, therefore the ratio of CO_2 to H_2O (C/H) in the heat carrier will also affect the C_2 yield.

In this work, the influence of the heat carrier composition on C_2 yield and selectivity were investigated in detail by both 0-dimensional (0-D) and three-dimensional (3-D) CFD simulations coupled with a detailed reaction mechanism. The heat carrier was changed by adding steam and adjusting the C/H ratio of the fuel gas, and their influences on the C_2 yield and selectivity were investigated by CFD simulations in the FIB reactor.

2. Computational Methods

The composition of heat carrier under stoichiometric combustion and with addition of steam were calculated by 0-D simulations under ideal mixing conditions. The 0-D simulations were also used to preliminarily optimize the reaction conditions for 3-D CFD simulations at a much lower computational cost. The 3-D CFD simulations were conducted to predict the C_2 yield and selectivity in a real reactor and were used to further optimize the operating conditions.

2.1. 0-D simulations

The simplified flow chart of the PDP is shown in Fig. 1. The 0-D simulations were carried out using CHEMKIN 18.0. The combustion of coke oven gas was simulated by the "closed homogeneous batch reactor" model, and the mixing of heat carrier and steam was simulated by the "non-reactive gas mixer" model. Before being mixed with ethane, the composition and temperature of heat carrier were recalculated by the "closed homogeneous batch reactor" model with addition of steam. Ethane is mixed with heat carrier and then undergoes pyrolysis at high temperature in "Reactor-2". The quenching process and the post processing were not discussed in this work.

2.2. 3-D CFD simulations

In the 0-D simulations, the mixing and pyrolysis processes are separated completely, while in a real reactor they occur simultaneously. Therefore, 3-D CFD simulations were carried to investigate the highly coupled mixing, chemical reactions, and heat transfer using ANSYS Fluent 16.0. The turbulence was described by the realizable k-ε model considering that it is more suitable than the standard k-ε model for jet flows with strong streamline curvature [24]. The realizable k-ε model satisfies mathematical constraints on Reynolds stresses and makes the calculation results realizable, because it contains an alternative formulation for turbulent viscosity. The calculation of the temperature and composition distributions near the wall was carried out by using standard wall functions, as the realizable k-ε model is not suitable for low turbulence conditions.

Conventional methods cannot describe the complex finite-rate chemical network well. The eddy-dissipation-concept (EDC) model was used to describe the interaction between turbulence and reaction, which has been successfully used in simulations of the methane POX process [25] and steam cracking process [26,27]. In addition, the computational cost and accuracy in combustions simulations can be balanced well by using the EDC model [28]. The in situ adaptive tabulation (ISAT) algorithm was used to reduce computational cost, which could accelerate the simulations by 2–3 orders of magnitude [29]. The discretized equations were solved by the steady implicit solver. The detailed settings of the CFD simulations are listed in Table 1.

2.3. Detailed reaction mechanism

In our previous works, the modified GRI 3.0 was validated [30] and was used to simulate the ethane PDP in an FIB reactor without steam addition [23]. This detailed reaction mechanism was also used in the present work to study the effect of adding steam to heat carrier. The original GRI 3.0 mechanism has been widely used in the calculations of C_1-C_3 combustion reactions [31]. To account for the fuel-rich characteristics, in the modified GRI 3.0 the rate

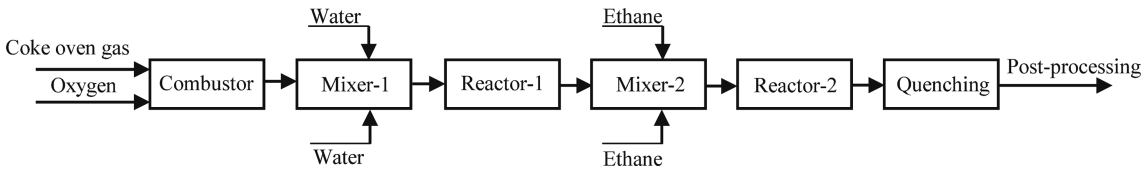

Fig. 1. Simplified flow chart of the PDP.

Table 1
Detailed settings of CFD simulations

Item	Settings
Solver	Steady, segregated with implicit formulation
Domain	Three-dimensional
Turbulence model	Realizable k-ε with default setting
Radiation	Discrete ordinates (DO) with Phi divisions = 5, Phi pixels = 3, Theta divisions = 5, Theta pixels = 3
Turbulence-chemistry interaction	Eddy dissipation concept (EDC) model with default parameters
Mixture material property	Absorption coefficient: wsggm-domain-based
Wall treatment	Standard wall functions
Discretization schemes	SIMPLE for pressure-velocity coupling, and Second order upwind for other equations
Under relaxation factors	Pressure: 0.3, density: 1.0, turbulent kinetic energy: 0.8, body forces: 1.0, momentum: 0.7, turbulent viscosity: 1, turbulent dissipation rate: 0.8, discrete ordinates: 1, species: 1
Convergence criteria	Equations of energy and Do-intensity: 10^{-6}; Equations of continuity, velocity, k, ε and species: 10^{-5}
Other options	Full multicomponent diffusion, thermal diffusion

constant of OH + C_2H_2 = CH_2CO + H was regressed based on experimental data as [25]:

$$k_{R1} = 1.326 \times 10^{13} T^{0.11} \exp(-11059RT) \quad (\mathrm{cm^3 \cdot mol^{-1} \cdot s^{-1}}) \qquad (1)$$

The modified GRI 3.0 used for simulating the conversion of ethane and the yields of acetylene and ethylene was verified in our previous work [21].

3. Numerical Settings

3.1. 0-D simulations

The molar composition of coke oven gas is set as 65% H_2, 25% CH_4, and 10% CO. The coke oven gas is preheated to 873 K and then combusts with stoichiometric oxygen, and then the product mixture is mixed with steam of 373 K and the composition and temperature are recalculated. Ethane is mixed with the heat carrier and undergoes pyrolysis under adiabatic conditions.

3.2. 3-D CFD simulations

3.2.1. Computational domain

The FIB reactor, which was demonstrated to have good performance in our previous work [23], is adopted to efficiently realize the ethane PDP with addition of steam. Typical parameters, including the inner diameter D_1, outer diameter D_2, and length of the reverse jet tubes, and diameter of the single computational unit D_3, are shown in Fig. 2. To reduce computational cost, a repeating unit of the whole reactor was used as the computational domain, with the side boundary condition set as "symmetry". The simulation results of the repeating unit and whole reactor were found to be similar in our previous work on scale-up effect of the FIB reactor. Fig. 3 shows the schematic map of FIB reactor mesh.

3.2.2. Boundary conditions

The heat carrier in this work was obtained by combustion of coke oven gas with stoichiometric oxygen and further mixing with steam of 373 K. The temperature and composition of heat carrier were calculated by 0-D simulations. The heat carrier without steam addition was fed into the reactor at a constant mass flow of 3.6 $kg \cdot h^{-1}$, and the mass flow of ethane was changed according to mixing ratio (φ), which was defined as the mass ratio of ethane to that of heat carrier without steam addition. The thermal boundary condition for the reverse jet tube was set as "coupled" between the flow and solid phases. The reactor outlet was set as pressure outlet. Other detailed settings of the FIB reactor are listed in Table 2.

3.2.3. Mesh independence test

In this section, the appropriate mesh density was investigated so that the computational cost can be reduced while keeping enough accuracy. Under the same mesh density, structural mesh could give better predictions than nonstructural mesh. Hence, structural mesh was used in the following simulations. Considering that the purpose of this work was to investigate the influence of changing the composition and temperature of heat carrier on the PDP of ethane in an FIB reactor, the mesh density used here was the same as that used in our previous work [23]. Therefore, the mesh with 495,697 nodes having mesh independence was adopted in this work.

4. Results and Discussion

The conversion of C_2H_6 and the selectivity and yield of major products are calculated by

$$C_2H_6 \text{ conversion} = \frac{F_{C_2H_6}}{F_{C_2H_6,0}} \qquad (2)$$

$$\text{Product yield} = \frac{z_i \times F_i}{2 \times F_{C_2H_6,0}} \qquad (3)$$

$$\text{Product selectivity} = \frac{z_i \times F_i}{2 \times (F_{C_2H_6,0} - F_{C_2H_6})} \qquad (4)$$

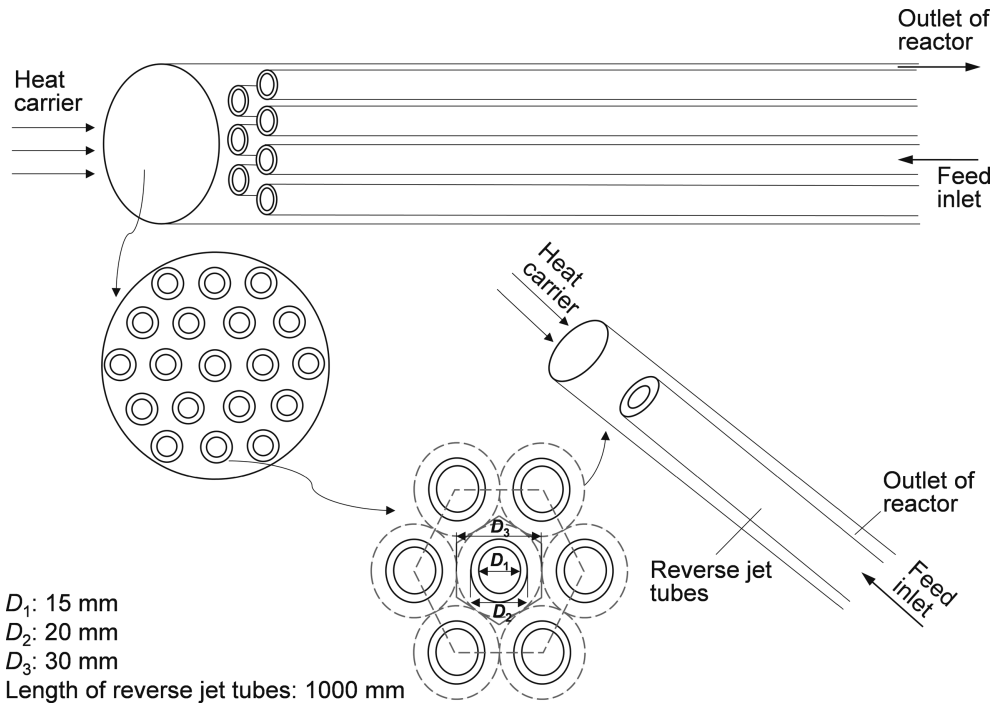

Fig. 2. Schematic structure of FIB reactor.

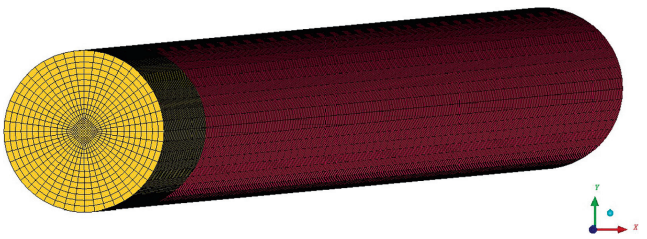

Fig. 3. Schematic map of FIB reactor mesh.

where F_i is the molar flow rate of species i, z_i is number of carbon atoms in molecule, and $F_{C_2H_{6,0}}$ is molar flow rate of C_2H_6 in feed. It should be noticed that the calculation of selectivity and yield is based on carbon atoms in C_2H_6. As the carbon atoms in heat carrier are almost converted to CO_2, they are not considered in the selectivity and yield calculations.

4.1. Adding steam to heat carrier

The temperature of coke oven gas combusting with stoichiometric oxygen could reach 3100 K. At such a high temperature, there is significant cracking of H_2O and CO_2. As listed in Table 3, the molar fractions of O_2, OH and O are 7.64%, 10.7% and 4.61%, respectively. For the PDP of ethane, the main byproducts are CH_4 and CO. The splitting reactions of C—C and C—H bonds are competitive. Because the bond energy of C—C is larger than that of C—H, a high temperature will promote the split of C—C and the formation of CH_3 and CH_2 radicals, and these radicals combine with H radical to generate CH_4 byproduct. During the pyrolysis process of ethane, hydrocarbons can be oxidized by O and OH radicals to oxygenate such as CH_3CO and CH_2CO, which will further compose to produce CO. Therefore, the CO yield can be reduced by decreasing the concentration of oxidizing radicals. Since the oxidizing radicals are produced by cracking of H_2O and CO_2 at high temperature, the key to increase the C_2 yield is to decrease the temperature of heat carrier. Steam is a promising candidate as it has a large specific heat capacity and does not introduce new substances. In addition, steam can be condensed into water easily at low temperatures, which is beneficial for separation.

The steam addition ratio β is defined as mass ratio of the added steam and the product of coke oven gas combustion with stoichiometric oxygen. The calculated molar fractions of main species of heat carrier with different steam addition are summarized in Table 3. With increasing addition of steam, the temperature and concentrations of oxidizing species decrease. When β = 1.8, the molar fractions of strongly oxidizing species such as O and O_2 decrease to ~0.01% and ~0.5%, respectively, and the molar fraction of OH decreases to 0.42%.

The cracking ratio C is defined as the ratio of cracked molecules to the original molecules without cracking. With increasing addition of steam, the temperature and cracking ratio of CO_2 and H_2O continue to decrease, as shown in Fig. 4. At β = 1.8, the cracking ratio of H_2O is close to 0, the cracking ratio of CO_2 is lower than 10%, and the temperature is lower than 2200 K. Further addition of steam does not significantly reduce the concentration of oxidizing species, but it decreases the temperature, which will decrease the reaction rate and increase the reaction time. Hence, the studied range of steam addition is 0–1.8 in this work. The cracking ratio of H_2O is much lower than that of CO_2, showing that H_2O is more stable than CO_2 at high temperatures and produces a lower amount of oxidizing species. The influence of the ratio of CO_2 to H_2O in heat carrier will be investigated in Section 4.3.

4.2. Influence of steam addition

4.2.1. 0-D simulations

Fig. 5 shows the simulation results of ethane PDP at different steam addition under ideal mixing conditions. As shown in Fig. 5 (a), when the steam addition ratio increases from 0 to 1.8, the yield of C_2 rises from 75.3% to 84.7%. The conversion of C_2H_6 is ~100% at different steam additions, indicating that the increase of C_2 yield is mainly attributed to the increased selectivity. As shown in Fig. 5 (b), with increasing steam addition, the CH_4 selectivity decreased from 16.1% to 11.8% and the CO selectivity decreases from 5.9% to 1.7%. The rapid decrease in CH_4 and CO selectivities confirms that it is feasible to increase C_2 yield by adding steam to the heat carrier to avoid excessively high temperature while providing enough heat for subsequent pyrolysis reactions.

In order to investigate the effect of addition steam in the heat carrier, the variation of the temperature and ethane concentration

Table 2
Detailed boundary conditions of the FIB reactor

Condition	Feed inlet	Heat carrier inlet
Mass flow/kg·h^{-1}	/	3.6 without steam addition
Temperature/K	873	3117 without steam addition
Turbulence intensity/%	10	10
Hydraulic diameter/mm	15	30
Radiation	Black body radiation of 300 K	Black body radiation of 300 K
Species composition	/	Adiabatic stoichiometric combustion results of coke oven gas from CHEMKIN simulation

Table 3
Molar fractions of main species in heat carrier with addition of steam

β	Molar fraction						Temperature/K
	O	O_2	OH	CO	CO_2	H_2O	
0	0.0461	0.0764	0.1070	0.1190	0.0655	0.417	3117
0.2	0.0245	0.0618	0.0836	0.0841	0.0730	0.546	2960
0.6	0.0072	0.0372	0.0459	0.0416	0.0785	0.719	2709
1.0	0.002	0.0206	0.0228	0.0193	0.0771	0.820	2495
1.4	5.1×10^{-4}	0.0104	0.0103	0.0082	0.0719	0.879	2299
1.8	1.1×10^{-4}	0.0049	0.0042	0.0031	0.0650	0.914	2118
2.2	2.1×10^{-5}	0.0021	0.0016	0.0011	0.0580	0.933	1954

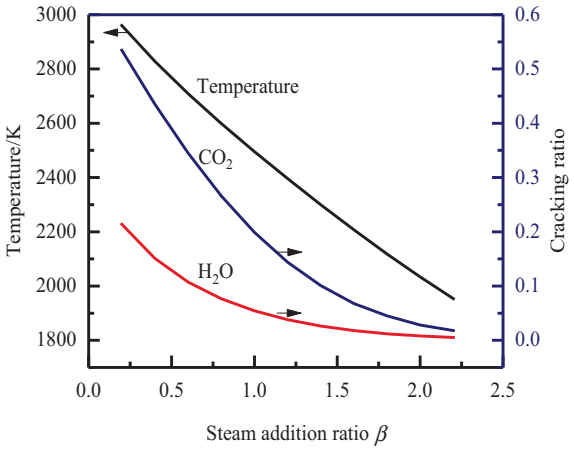

Fig. 4. The temperature and cracking ratios of CO_2 and H_2O at different steam addition.

with reaction time under ideal mixing conditions are compared for β = 0 and 1.4, as shown in Fig. 6. It can be seen from Fig. 6(a) that ethane converts slowly at β = 1.4 due to the low concentration of strong oxidizing species. The conversion of ethane starts at 10^{-6} s and 10^{-8} s at β = 1.4 and 0, respectively. Thus the requirement of fast mixing decreases with steam addition. The temperature profiles at β = 0 and β = 1.4 are shown in Fig. 6(b). The temperature without steam addition (β = 0) increases initially and then decreases since some ethane is oxidized by strong oxidizing species in the initial period. With steam addition (β = 1.4), the temperature keeps decreasing with reaction time due to endothermic reactions of ethane pyrolysis and low concentration of strong oxidizing species. Note that the variation of temperature is similar at β = 0 and 1.4 after 10^{-6} s of reaction.

4.2.2. CFD simulations

The 0-D simulation results show that the C_2 yield can be improved by adding steam to the heat carrier. The ethane PDP with steam addition is further studied by CFD simulations in a FIB reactor. Fig. 7 shows the comparison between CFD and 0-D simulation results. As shown in Fig. 7(a), with the increase of steam addition, the difference of C_2 yield between 0-D simulations at ideal mixing and 3-D CFD simulations becomes smaller. At ideal mixing conditions, the C_2 yield is 75.3% without steam addition and it is 82.9% at steam addition ratio of 1.4. In comparison, the C_2 yield in an FIB reactor is 62.4% without steam addition and it increases to 78.5% with steam addition (β = 1.4). The difference in C_2 yields between ideal mixing and FIB reactor is much smaller at β = 1.4 than that at β = 0. This is because the concentration of strong oxidizing species and reaction temperature decrease with increasing steam addition. Furthermore, the addition of steam decreases the reaction rate of C_2H_6, which lowers the demand for high mixing efficiency. For further investigation, the yields of CH_4 and CO are shown in Fig. 7(b). The difference of CH_4 yield between 0-D and CFD simulations is similar at different steam addition ratios, while the difference of CO yield decreases significantly with increasing addition of steam, showing that CO formation is much more sensitive to mixing efficient than CH_4 formation. In the CFD simulation results, the CO yield decreases from 16.1% with steam addition to 4.6% at β = 1.4, which contribute the significant increase in C_2 yield.

The mixing ratio is defined as the mass flow ratio between heat carrier without steam addition and ethane feed. It will significantly affect the chemical reactions by changing temperature of the system. The amount of oxidizing species and the pyrolysis temperature decrease with an increase in the mixing ratio. Fig. 8 shows the effects of the mixing ratio on the conversion of C_2H_6, selectivity to C_2 and yields of C_2H_2 and C_2H_4. As shown in Fig. 8(a), the C_2 yield reaches its maximum of 74.2% at a mixing ratio of 1.2 and steam addition ratio β = 1.0. With the increase of mixing ratio, the conversion of C_2H_6 decreases while the C_2 selectivity increases, due to lower concentration of oxidizing species. However, the fractions of C_2H_2 and C_2H_4 significantly change with the mixing ratio. The yield of C_2H_2 decreases while that of C_2H_4 increases with the increase of mixing ratio. The major product is C_2H_2 at low mixing ratios while it is C_2H_4 at high mixing ratios. For example, the C_2H_2 and C_2H_4 yields are respectively 47% and 24.4% at a mixing ratio of 0.8, while they are 14.7% and 57%, respectively, at a mixing ratio of 1.4. This is because C_2H_2 is more stable than C_2H_4 under high temperature. With steam addition at β = 1.4, as shown in Fig. 8(b), the C_2 yield reaches its maximum of 78.5% at a mixing ratio of 1.1. With the increase of mixing ratio, the conversion of C_2H_6 decreases and the C_2 selectivity increases, which is similar to that at β = 1.0.

The jetting velocity of heat carrier affects the turbulence energy greatly during the mixing process, and its effect was studied by adjusting the flow rate of the heat carrier without steam addition while keeping the mixing ratio at 1.1 and steam addition ratio at 1.4. Fig. 9 shows that the C_2H_6 conversion and

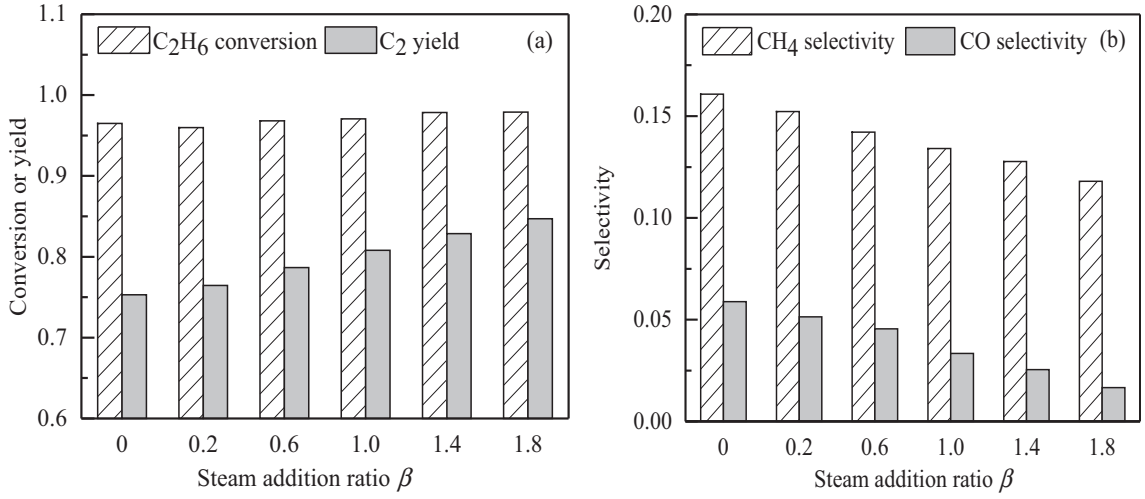

Fig. 5. Simulation results of ethane PDP at different steam additions under ideal mixing conditions: (a) C_2H_6 conversion and C_2 (C_2H_2 + C_2H_4) yield; (b) selectivities of CH_4 and CO.

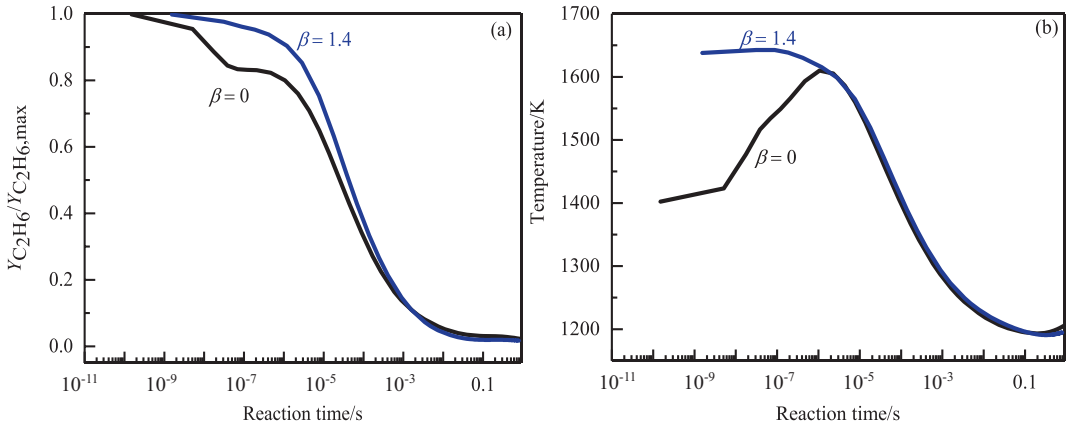

Fig. 6. Effect of steam addtion on the variation of (a) normalized mass fraction of C_2H_6 and (b) temperature with reaction time under ideal mixing conditions.

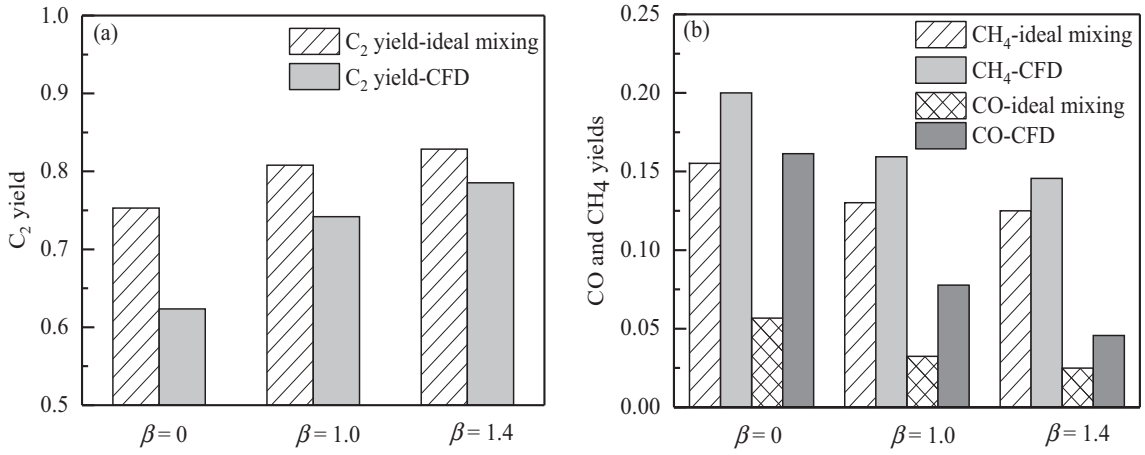

Fig. 7. Comparison of 0-D and 3-D CFD simulation results of (a) C_2 yield and (b) CH_4 and CO yield at different steam addition ratios.

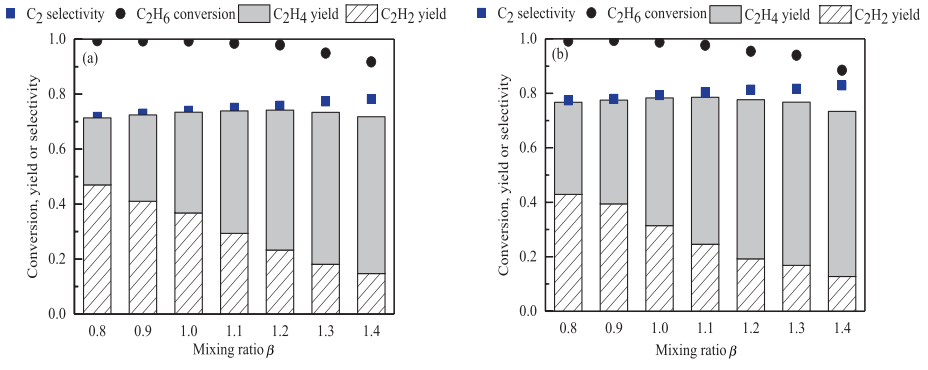

Fig. 8. Effect of mixing ratio on C_2H_6 conversion, C_2 selectivity and yields of C_2H_2 and C_2H_4 (a) β = 1.0 and (b) β = 1.4.

C_2H_2 and C_2H_4 selectivities are insensitive to the heat carrier jetting velocity. Considering the pressure drop, the maximum of the jetting velocity is set as ~100 m·s^{-1}. As shown in Fig. 9(a), the C_2 yield increases from 78.7% to 79.9%. The C_2 selectivity also rises slightly from 80% to 81.4% and the C_2H_6 conversion remains at ~98% in all cases. The C_2 yield increases with the increase of jetting velocities due to enhanced mixing. This is why the C_2 yield in 0-D simulations is higher than in 3-D CFD simulation. To further discuss the influence of the jetting velocity of heat carrier, the yields of CH_4 and CO are shown in Fig. 9(b). The CO yield decreases slightly from 4.6% to 3.5% as the jetting velocity increases from 34 to 97 m·s^{-1}, while the CH_4 yield is almost unchanged. The high jetting velocity, which makes the oxidizing species distribute more uniformly, decreases the CO yield, because the generation of CO is more sensitive to mixing efficiency than that of CH_4.

4.3. Influence of C/H in hear carrier

The molar fraction of the fuel gas in our previous work was set as 65% H_2, 25% CH_4, and 10% CO. The cracking ratio of H_2O and CO_2 in the combustion product mixture is different, as shown in Fig. 4,

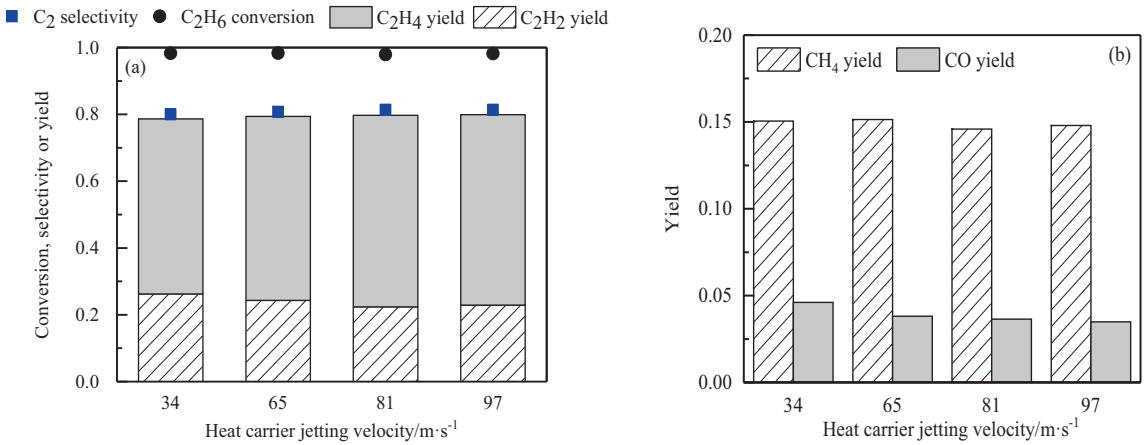

Fig. 9. Effect of heat carrier jetting velocity on (a) C_2H_6 conversion and C_2 (C_2H_2 + C_2H_4) yield and selectivity, and (b) yields to CO and CH_4.

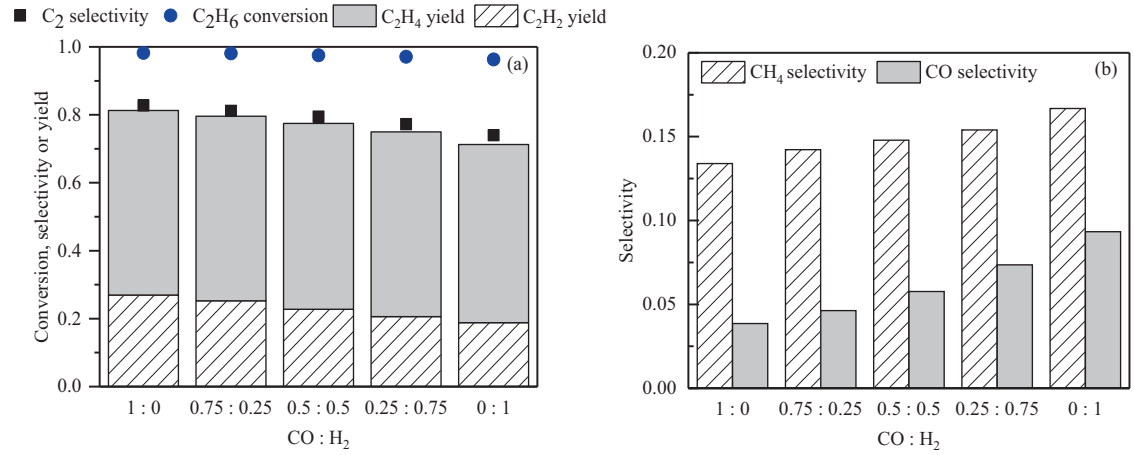

Fig. 10. Effect of different CO/H_2 ratios in the fule gas on (a) C_2H_6 conversion and C_2 (C_2H_2 + C_2H_4) yield and selectivity and (b) selectivity to byproducts CO and CH_4.

leading to different concentrations of oxidizing species. The influence of C/H in fuel was studied by setting the fuel as a mixture of CO and H_2 and changing their ratio at constant operating conditions.

The fuel gas combusts with stoichiometric oxygen and then mixed with steam addition ratio β = 1.0. Ethane is mixed with the heat carrier and the maximum C_2 yield is obtained by changing the mixing ratio. Fig. 10 shows the 3-D CFD simulation results at different C/H ratios. It can be seen from Fig. 10(a) that the C_2 yield decreases from 81.3% when pure CO was used as fuel gas to 71.2% with pure H_2 as fuel gas. At different C/H ratios, the C_2H_6 conversion is close to 100%, while the C_2 selectivity decreases with decreasing C/H. The main reason is that the calorific value of H_2 is larger than that of CO, and the temperature of heat carrier increases from 2138 K with pure CO to 2633 K with pure H_2.

Under high temperatures, ethane splits into CH_3 radicals, which will produce CH_4 by reacting with H radicals [32]. Thus the increase of temperature promotes the formation of CH_4 and reduces the yield of C_2. As discussed in Section 4.1, at a high temperature of heat carrier more oxidizing species is generated, leading to enhanced formation of CO. Fig. 10(b) shows that the selectivity of byproducts increases with an increase in H_2 proportion in the gas fuel. Therefore, a higher steam addition ratio is needed when the H_2 proportion in the fuel is increased to lower the temperature of the heat carrier.

5. Conclusions

The influence of changing the heat carrier composition on the partially decoupled process of ethane was investigated by simulations with detailed chemistry. The heat carrier was changed by adding steam and adjusting the C/H ratio of the gas fuel to enhance the C_2 yield. By adding steam to the heat carrier, the molar fraction of strong oxidizing species decreases from ~10^{-2} to ~10^{-3}. In the heat carrier, H_2O is more stable than CO_2 at high temperature, having a lower cracking ratio and produces a lower amount of oxidizing species. At ideal mixing conditions, the C_2 yield increases from 75.3% without steam addition to 84.7% at steam addition ratio of β = 1.8, because steam addition decreases both CO and CH_4 yields. CFD simulations of an FIB reactor shows that the maximum C_2 yields at β = 1.0 and 1.4 are 74.2% and 78.5%, respectively. The requirement of high mixing efficiency is diminished by steam addition, which is favorable for reactor scale-up. With increasing H_2 proportion in gas fuel, C_2 yield decreases and a higher steam addition is needed to lower the temperature of heat carrier.

Declaration of Competing Interest

The authors declare that they have no known competing financial interests or personal relationships that could have appeared to influence the work reported in this paper.

Acknowledgements

This work was supported by the National Natural Science Foundation of China (21276135), and by Project of Chinese Ministry of Education (113004A).

References

[1] Z.R. Chong, S.H.B. Yang, P. Babu, P. Linga, X. Sen Li, Review of natural gas hydrates as an energy resource: Prospects and challenges, *Appl. Energy* 162 (2016) 1633–1652.
[2] H.J. Eom, S. HeeAn, B.H. Chon, Evaluation of shale gas reservoirs considering the effect of fracture half-length and fracture spacing in multiple hydraulically fractured horizontal wells, *Geosyst. Eng.* 17 (5) (2014) 264–278.
[3] M. Shah, S. Shah, A. Sircar, A comprehensive overview on recent developments in refracturing technique for shale gas reservoirs, *J. Nat. Gas Sci. Eng.* 46 (2017) 350–364.
[4] J.J.H.B. Sattler, J. Ruiz-Martinez, E. Santillan-Jimenez, B.M. Weckhuysen, Catalytic dehydrogenation of light alkanes on metals and metal oxides, *Chem. Rev.* 114 (20) (2014) 10613–10653.
[5] D. Dong, Y. Wang, X. Li, C. Zou, Q. Guan, C. Zhang, J. Huang, S. Wang, H. Wang, H. Liu, W. Bai, F. Liang, W. Lin, Q. Zhao, D. Liu, Z. Qiu, Breakthrough and prospect of shale gas exploration and development in China, *Nat. Gas Ind. B.* 3 (1) (2016) 12–26.
[6] M. Finkel, J. Hays, A. Law, The shale gas boom and the need for rational policy, *Am. J. Public Health.* 103 (7) (2013) 1161–1163.
[7] A. Galadima, O. Muraza, Revisiting the oxidative coupling of methane to ethylene in the golden period of shale gas: A review, *J. Ind. Eng. Chem.* 37 (2016) 1–13.
[8] H. Hu, W. Wei, C.P. Chang, Do shale gas and oil productions move in convergence? An investigation using unit root tests with structural breaks, *Econ. Model.* 77 (2019) 21–33.
[9] Q. Wang, X. Chen, A.N. Jha, H. Rogers, Natural gas from shale formation - The evolution, evidences and challenges of shale gas revolution in United States, *Renew. Sustain. Energy Rev.* 30 (2014) 1–28.
[10] J.J. Siirola, The impact of shale gas in the chemical industry, *AIChE J.* 60 (3) (2014) 810–819.
[11] S.M. Sadrameli, Thermal/catalytic cracking of hydrocarbons for the production of olefins: A state-of-the-art review I: Thermal cracking review, *Fuel* 140 (2015) 102–115.
[12] M.K. Sabbe, K.M. Van Geem, M.-F. Reyniers, G.B. Marin, First principle-based simulation of ethane steam cracking, *AIChE J.* 57 (2) (2011) 482–496.
[13] S.M. Sadrameli, Thermal/catalytic cracking of liquid hydrocarbons for the production of olefins: A state-of-the-art review II: Catalytic cracking review, *Fuel* 173 (2016) 285–297.
[14] A.S. Al-Awadi, A.M. El-Toni, S.M. Al-Zahrani, A.E. Abasaeed, M. Alhoshan, A. Khan, J.P. Labis, A. Al-Fatesh, Role of TiO_2 nanoparticle modification of Cr/MCM41 catalyst to enhance Cr-support interaction for oxidative dehydrogenation of ethane with carbon dioxide, *Appl. Catal. A Gen.* 584 (2019) 117114.
[15] M. Hurtado Cotillo, D. Unsihuay, C.E. Santolalla-Vargas, A. Paredes Doig, R. Sun Kou, G. Picasso, Catalysts based on Ni-Fe oxides supported on γ-Al_2O_3 for the oxidative dehydrogenation of ethane, *Catal. Today*. 356 (2020) 312–321.
[16] B. Fu, J. Lu, P.C. Stair, G. Xiao, M.C. Kung, H.H. Kung, Oxidative dehydrogenation of ethane over alumina-supported Pd catalysts. Effect of alumina overlayer, *J. Catal.* 297 (2013) 289–295.
[17] C.A. Gärtner, A.C. vanVeen, J.A. Lercher, Oxidative dehydrogenation of ethane: Common principles and mechanistic aspects, *ChemCatChem* 5 (2013) 3196–3217.
[18] S.F. Håkonsen, J.C. Walmsley, A. Holmen, Ethene production by oxidative dehydrogenation of ethane at short contact times over Pt-Sn coated monoliths, *Appl. Catal. A Gen.* 378 (1) (2010) 1–10.
[19] L. Ji, J. Liu, X. Chen, M. Li, Effect of group VIII elements on the behavior of Li/CaO catalyst in the oxidative dehydrogenation of ethane, *React. Kinet. Catal. Lett.* 62 (1) (1997) 121–128.
[20] Q. Zhang, J. Wang, T. Wang, Enhancing the acetylene yield from methane by decoupling oxidation and pyrolysis reactions: A comparison with the partial oxidation process, *Ind. Eng. Chem. Res.* 55 (2016) 8383–8394.
[21] Q. Zhang, J. Luo, T. Chen, J. Wang, T. Wang, Enhancement of the acetylene and ethylene yields from ethane by partially decoupling the oxidation and pyrolysis reactions, *Chem. Eng. Process. Process Intensif.* 122 (2017) 447–459.
[22] J. Luo, J. Wang, T. Wang, Experimental study of partially decoupled oxidation of ethane for producing ethylene and acetylene, *Chin. J. Chem. Eng.* 26 (6) (2018) 1312–1320.
[23] J. Luo, J. Wang, T. Wang, A new forward-impinging-back reactor for the scale-up of partially decoupled oxidation of ethane to produce ethylene and acetylene, *Chem. Eng. Process. - Process Intensif.* 145 (2019) 107646.
[24] T.-H. Shih, W.W. Liou, A. Shabbir, Z. Yang, J. Zhu, A new k-ε eddy viscosity model for high reynolds number turbulent flows, *Comput. Fluids.* 24 (3) (1995) 227–238.
[25] Q. Zhang, Y. Liu, T. Chen, X. Yu, J. Wang, T. Wang, Simulations of methane partial oxidation by CFD coupled with detailed chemistry at industrial operating conditions, *Chem. Eng. Sci.* 142 (2016) 126–136.
[26] G.D. Stefanidis, B. Merci, G.J. Heynderickx, G.B. Marin, CFD simulations of steam cracking furnaces using detailed combustion mechanisms, *Comput. Chem. Eng.* 30 (4) (2006) 635–649.
[27] G. Hu, C.M. Schietekat, Y. Zhang, F. Qian, G. Heynderickx, K.M. Van Geem, G.B. Marin, Impact of radiation models in coupled simulations of steam cracking furnaces and reactors, *Ind. Eng. Chem. Res.* 54 (9) (2015) 2453–2465.
[28] I.S. Ertesvag, B.F. Magnussen, The eddy dissipation turbulence energy cascade model, *Combust. Sci. Technol.* 159 (1) (2000) 213–235.
[29] S.B. Pope, Computationally efficient implementation of combustion chemistry using *in situ* adaptive tabulation, *Combust. Theory Model.* 1 (1997) 41–63.
[30] Y. Liu, Q. Zhang, T. Wang, Detailed chemistry modeling of partial combustion of natural gas for coproducing acetylene and syngas, *Combust. Sci. Technol.* 189 (5) (2017) 908–922.
[31] D.M.G. Gregory, P. Smith Michael Frenklach, N.W. Moriarty, B. Eiteneer, M. Goldenberg, C. Thomas Bowman, R.K. Hanson, S. Song, W.C. Gardiner Jr., V.V. Lissianski, Z. Qin, The GRI 3.0 mechanism, (2008), http://www.me.berkeley.edu/gri_mech/.
[32] M.W.M. van Goethem, S. Barendregt, J. Grievink, P.J.T. Verheijen, M. Dente, E. Ranzi, A kinetic modelling study of ethane cracking for optimal ethylene yield, *Chem. Eng. Res. Des.* 91 (6) (2013) 1106–1110.